PROCEEDINGS OF ECOS 2023 - THE 36TH INTERNATIONAL CONFERENCE ON
EFFICIENCY, COST, OPTIMIZATION, SIMULATION AND ENVIRONMENTAL IMPACT OF ENERGY SYSTEMS
25-30 JUNE, 2023, LAS PALMAS DE GRAN CANARIA, SPAIN

Online model-based framework for operation and fouling monitoring in a large-scale heat pump

José Joaquín Aguilera [a], Wiebke Meesenburg [a], Wiebke Brix Markussen [b], Benjamin Zühlsdorf [b] and Brian Elmegaard [a]

[a] Department of Civil and Mechanical Engineering, Technical University of Denmark, Kgs. Lyngby, 2800, Denmark, jojap@mek.dtu.dk
[b] Danish Technological Institute, Aarhus C, 8000, Denmark, bez@teknologisk.dk

Abstract:

Heat pump systems are a key technology towards the decarbonisation of district heating systems as they can leverage renewable energy sources and industrial excess heat. Large-scale heat pumps are prone to a variety of faults related to the heat source. Heat exchanger fouling is one of the most common types of faults, which corresponds to the undesired deposition of material on heat transfer surfaces. This fault can be mitigated by the use of different cleaning procedures such as cleaning-in-place. The optimization of the time interval between cleaning periods requires the estimation of the effects of fouling on the heat pump performance, which are often difficult to determine. The present study proposes a framework for online monitoring of a large-scale heat pump affected by evaporator fouling based on a quasi-steady-state simulation model. Model parameters related to the heat transfer coefficients and fouling were repeatedly adjusted by means of a dynamic calibration approach. The framework retrieved operational data from a cloud-based data management system and leveraged existing sensors and controllers in the heat pump. The results indicated that fouling had a larger effect on the thermal resistance than on the pressure drop in the evaporator. The framework also allowed to identify the extent to which a cleaning-in-place system enabled to reduce the evaporator thermal resistance caused by fouling. Overall, the results from the proposed framework showed its potential to describe the operation of the heat pump and to determine the effects of fouling on a real-time basis.

Keywords:

Heat pump, District heating, Fouling, Operation monitoring, Digital twin

1. Introduction

Heat pumps (HPs) are expected to play a major role in the decarbonisation of district heating systems. Today, around 90 % of the global heat supply derives from fossil fuels [1]. HPs enable waste heat recovery and utilization of renewable energy sources. Further, they couple the power and heating sectors, which can support the accommodation of large shares of electric energy from renewable sources in the system. The performance and/or availability of HPs is often negatively affected by faults related to the heat source, as described by HP operators and service providers in [2]. A literature study [3] distinguished fouling in the source side of heat exchangers to be among the most common faults in large-scale HPs. This fault consists of the deposition of material on heat transfer surfaces and in pipes, which can increase the pressure drop and thermal resistance in heat exchangers. As mentioned in [4], the characterization of fouling is challenging, particularly due to uncertainties on the initialization of the deposition process and its growth rate.

Commonly used technologies for the mitigation of fouling are cleaning-in-place (CIP) systems. These include mechanical and chemical cleaning processes [5], which are often off-line i.e. are applied while the heat pump is not in operation. Hence, finding the optimal moment and duration of the CIP activation represents a techno-economic optimization problem. This requires information about the extent to which a particular CIP is able to remove the deposited material as well as information about downtime and CIP implementation costs. A study [6] highlighted the challenge of predicting the thermal resistance attributed to fouling in the source stream heat exchanger of a large-scale wastewater heat pump. This study used data-driven regression models for the prediction of the thermal resistance caused by fouling. The data-driven regressions model were designed for the purpose of optimizing the cleaning procedures.

Physics-based simulation models are useful for the design of HPs and their components, mainly because they are applicable to a wide variety of boundary conditions and system configurations. However, the structure and parametrisation of such models is often fixed and does not adapt to time-dependent variations in the HPs they

https://doi.org/10.52202/069564-0296

represent. Such variations can be caused by faults or wear of components. In order to overcome this limitation, physics-based models may be complemented with numerical models derived from observations or data-driven models for the provision of services for HPs. Examples of such services include fault detection and diagnosis [7,8], operation monitoring [9], and defrosting optimization [10].

The provision of model-based services for HPs used for district heating supply still remains limited. A model-based monitoring and optimization framework has the potential to characterize the operation of a HP for a wide range of operational conditions and identify parameters that could enhance the HP performance. In particular, a thermodynamic model that could adapt its structure based real-time monitored data may enable the characterization of incipient faults affecting the HP, which has not been found in previous studies. The present study aimed at the increase of a HP performance through an improved CIP planning procedure characterized by an automatic model calibration framework. This framework was based on the integration of a physics-based model of the HP with data-driven optimization methods for model calibration.

2. Method

2.1. Case study heat pump

The operation of a two-stage ammonia HP with a design heating capacity of 2 MW was analysed in this study and its layout is shown in Figure 1. The HP is used for the provision of heat at around 68 °C to a local district heating network located in Copenhagen, Denmark. The heat source is industrial wastewater at around 23 °C originated from a biochemical plant. The desuperheater (DSH), condenser, receiver and subcooler (SC) are embedded in a single shell-and-plate heat exchanger unit. The evaporator is also a shell-and-plate heat exchanger and is in direct contact with the industrial wastewater. Each of the two stages in the HP includes a reciprocating compressor and an electronic expansion valve. An open intercooler connects both stages. The HP is controlled by means of the six controllers shown in Figure 1.

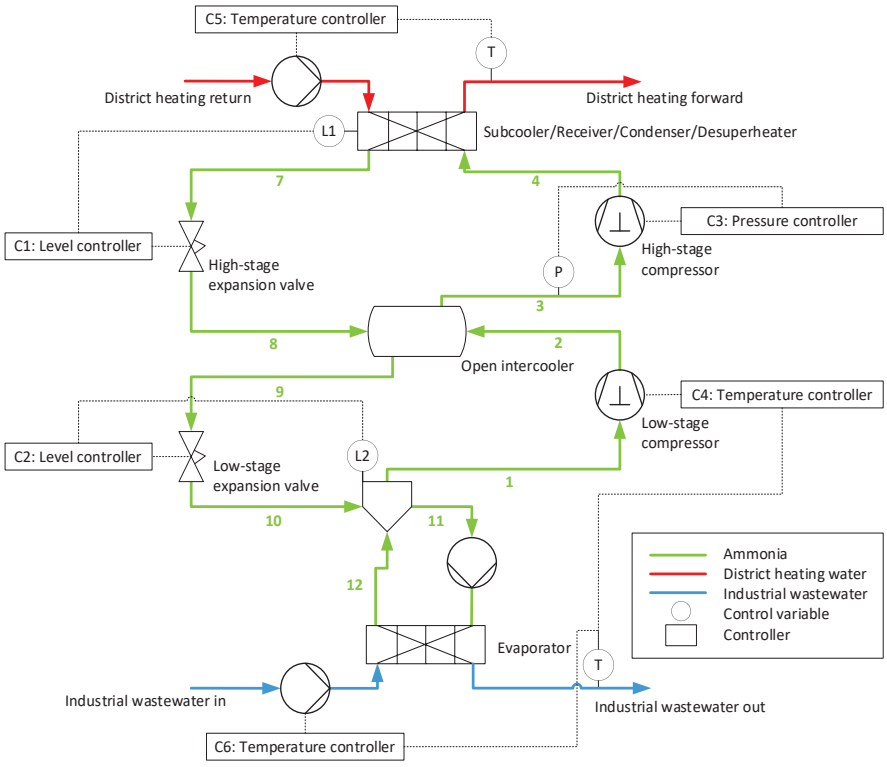

Figure 1: Layout of the two-stage ammonia HP used as case study

The direct contact between the industrial wastewater and the evaporator leads to the presence of fouling in this component, which is mitigated periodically by means of a CIP system. The CIP is used off-line and circulates a chemical solution for the removal of deposited inorganic and organic materials. These materials derived from the industrial processes performed in the biochemical plant. Currently, the frequency of the CIP implementation is defined heuristically by the HP operator based on observations on a decrease in the evaporation pressure (p_e).

https://doi.org/10.52202/069564-0296

2.2. Simulation model

The quasi-steady-state model of the HP shown in Figure 2 was developed in the programming language Python. The model took as input variables the source inlet and outlet temperatures ($T_{source,in}$ and $T_{source,out}$, respectively), the sink inlet temperature ($T_{sink,in}$), the set point for the intermediate pressure ($p_{m,sp}$) as well as the volume flow rates in the source and sink streams (V_{source} and V_{sink}, respectively). The refrigerant states and mass flow rates, heat output and power intake from the HP were determined through an iteration routine that solved the mass and energy balances of the components shown in Figure 2. This was done by the Newton-Raphson method with a tolerance of 10^{-9}, which identified the condensation and intermediate and pressures (p_c, and p_m, respectively), as well as the speed of the low-stage (LS) compressor (N_{LS}). Here, the residuals were the difference between the estimated and real area of the condenser ($A_{cond,calc}$ and A_{cond}), the estimated and real cooling capacity ($\dot{Q}_{source,calc}$ and $\dot{Q}_{source}$) and the LS mass flow rate estimated from the intercooler and the LS compressor models ($\dot{m}_{LS,IC}$ and $\dot{m}_{LS}$). An upper level iteration process enabled to identify the speed of the high-stage (HS) compressor that led to a minimum difference between the intermediate pressure (p_m) and its set point ($p_{m,sp}$). This was performed by the least-squares method with a tolerance of 10^{-5}. The Python module SciPy [11] was used for the implementation of the least-squares method. The refrigerant state calculations were performed with the Coolprop database [12]. The simulation of the quasi-steady-state model was done through multiprocessing, where 10 processing units were used in parallel within a single computer. Here, a simulated period was divided into 10 segments. All segments were simulated by different processors and the guess values were adjusted dynamically within each processor, namely the simulation results from a point in time *i* were used as guess values for the following point *i*+1. As a reference, the simulation of one hour of HP operation (i.e. 60 one-minute data points) required approximately 10 seconds when using multiprocessing an dynamically adjusted guess values, whereas it took around 113 seconds with a single processor and fixed guess values.

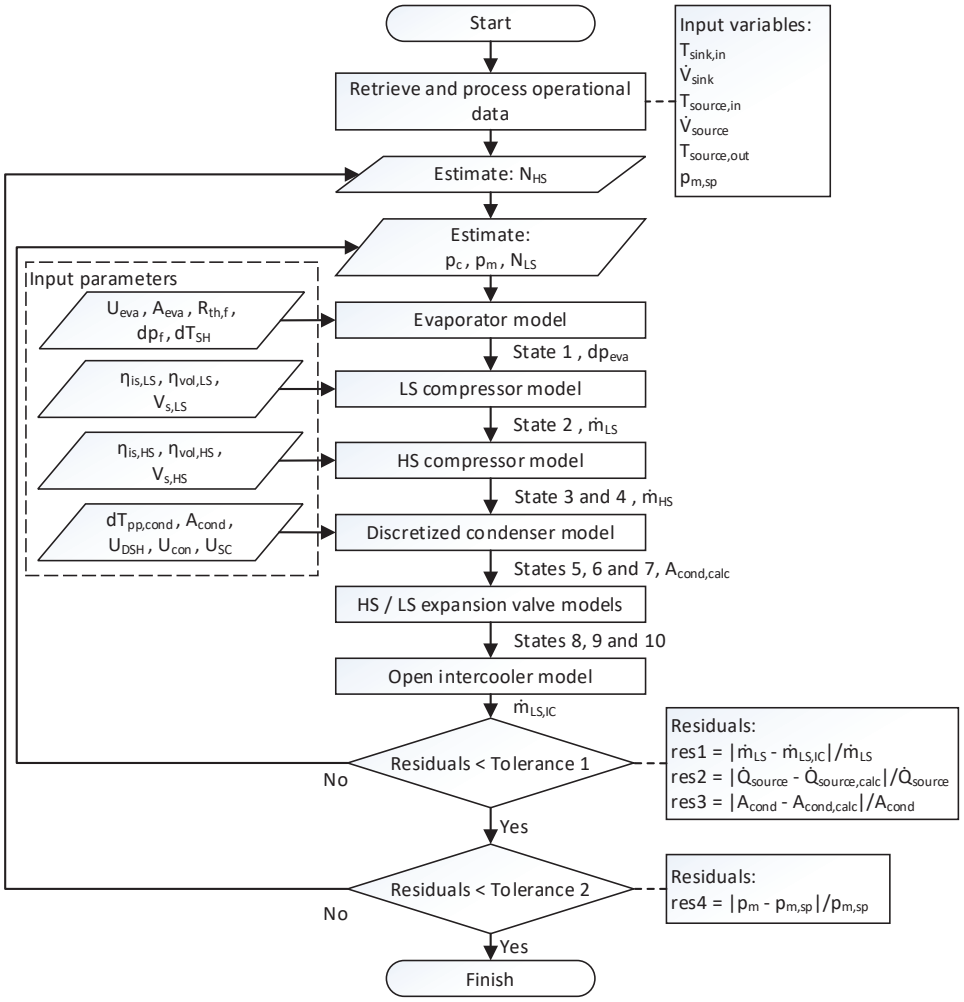

Figure 2: Flow diagram of the HP simulation model

The thermal resistance ($R_{th,f}$) and source stream pressure drop due to fouling (dp_f) were included as input parameters in the evaporator, which were later adjusted based on measurements through the calibration process described in Section 2.3.2. The $R_{th,f}$ was calculated based on Eq. (1), where the thermal resistance of the evaporator under clean conditions ($R_{th,eva,clean}$) was subtracted to the total thermal resistance ($R_{th,eva}$). Both thermal resistances were obtained as the inverse of the UA-value of the evaporator. Similarly, dp_f was determined based on Eq. (2) as the total pressure drop in the evaporator source side (dp_{eva}) minus the source stream pressure drop that was not caused by fouling ($dp_{eva,clean}$). The latter was determined by fitting a quadratic regression model between the volume flow rate in the source stream and the pressure drop in the evaporator right after the CIP was applied. Thereby, the influence of fouling was neglected in such a regression model.

$$R_{\mathrm{th,f}} = 1/\mathrm{UA}_{\mathrm{eva}} - 1/\mathrm{UA}_{\mathrm{eva,clean}} = R_{\mathrm{th,eva}} - R_{\mathrm{th,eva,clean}} \quad (1)$$

$$dp_{\mathrm{f}} = dp_{\mathrm{eva}} - dp_{\mathrm{eva,clean}} \quad (2)$$

The design parameters used in the model are shown in Table 1 and were provided by the HP manufacturer. , the pinch point temperature difference in the condenser ($dT_{pp,cond}$) was assumed to be 5 K. The isentropic and volumetric efficiencies of the compressors (η_{is} and η_{vol}, respectively) were calculated as a function of the compressor speed and the pressure ratios by using polynomials that were determined from information provided by the HP manufacturer.

Table 1: Input parameters used in the simulation model

Component	Input parameter	Symbol	Value	Unit
DSH	Overall heat transfer coefficient	U_{DSH}	230	W/m²K
	Heat transfer area	A_{DSH}	27.8	m²
Condenser	Overall heat transfer coefficient	U_{con}	1210	W/m²K
	Heat transfer area	A_{con}	100.6	m²
	Pinch point temperature difference	$dT_{pp,cond}$	5	K
SC	Overall heat transfer coefficient	U_{SC}	452	W/m²K
	Heat transfer area	A_{SC}	23.1	m²
Evaporator	Overall heat transfer coefficient	U_{eva}	3000	W/m²K
	Heat transfer area	A_{eva}	91.96	m²
	LS suction superheat	dT_{SH}	1	K
Low-stage compressor	Swept volume	$V_{s,LS}$	1018	m³/rev
	Speed	N_{LS}	700-1800	rpm
High-stage compressor	Swept volume	$V_{s,HS}$	532	m³/rev
	Speed	N_{LS}	700-1800	rpm

After the calculation of all the refrigerant states and water outlet temperatures, the model calculated the total heat output ($\dot{Q}_{sink}$) and the coefficient of performance (COP) of the HP based on Eq. (3) and Eq. (4). Here, it was assumed that the specific heat capacity ($c_{p,w}$) and density of water (ρ_w) were constant and equal to 4.18 kJ/(kg·K) and 998 kg/m³, respectively.

$$\dot{Q}_{\mathrm{sink}} = c_{\mathrm{p,w}} \cdot \rho_{\mathrm{w}} \cdot \dot{V}_{\mathrm{sink}} \cdot (T_{\mathrm{sink,out}} - T_{\mathrm{sink,in}}) \quad (3)$$

$$\mathrm{COP} = \dot{Q}_{\mathrm{sink}} / \dot{W}_{\mathrm{total}} \quad (4)$$

2.3. Monitoring framework

The framework proposed in this study consisted of the main components presented in Figure 3. Data from the HP controllers and sensors was accessed by the HP operator through a supervisory control and data acquisition (SCADA) system. The data from the SCADA system was made available to third-party actors through a cloud data management system, which enabled the storage and retrieval of operational data in real-time through an application programming interface (API). Such operational data from the HP was used to calibrate the simulation model described in Section 2.2.

https://doi.org/10.52202/069564-0296

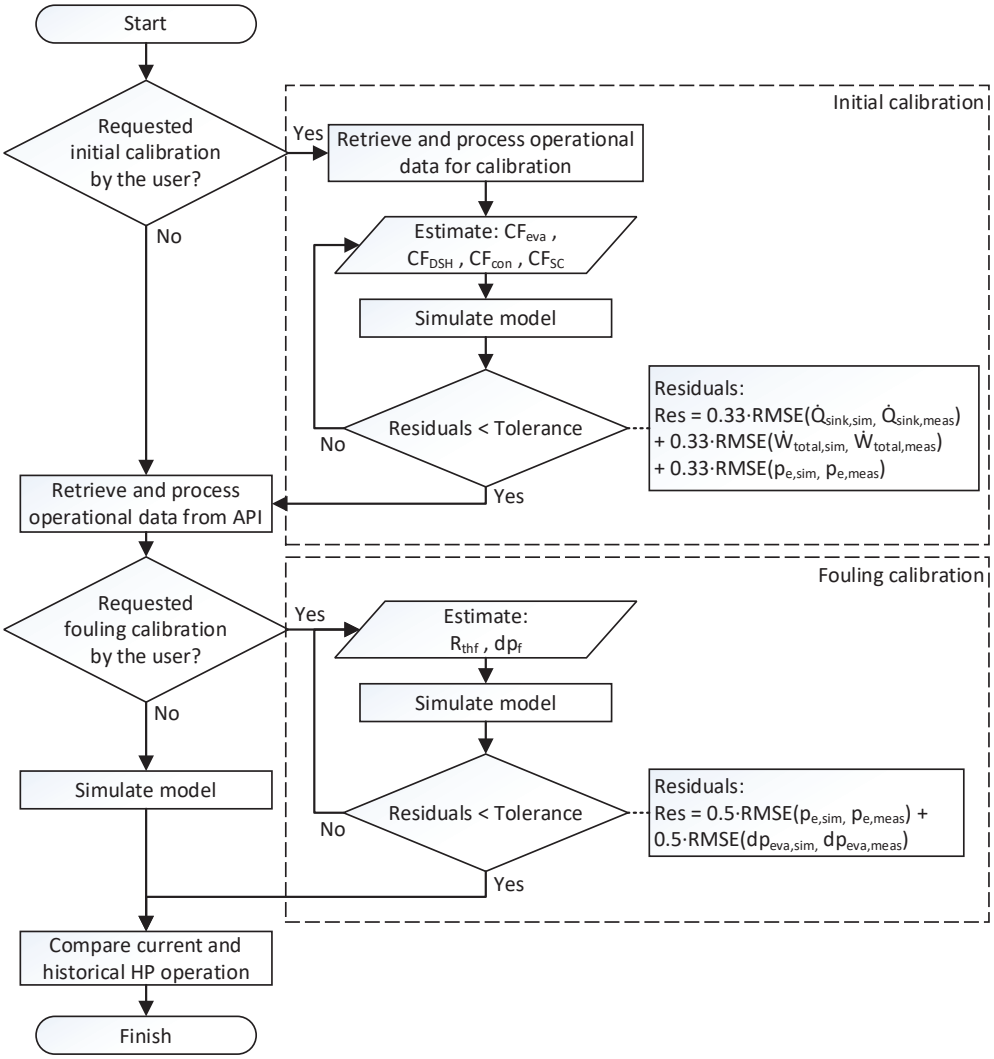

Figure 3: Flow diagram of the proposed monitoring framework

2.3.1. Data retrieval and processing

In the present study, the operational data from the case study HP was retrieved with a one-minute interval. The retrieval and processing of data was performed through Python. Here, the data processing consisted on the calculation of all the refrigerant states shown in Figure 1, for which the Coolprop database was used. This allowed to determine the COP and $\dot{Q}_{sink}$ from the HP by the use of Eq. (3) and Eq. (4). The total operational period included in the present study was 19 days. That period incorporated the activation of the existing CIP system for approximately 3 days, where the HP was not in operation.

2.3.2. Model calibration

Two calibration processes were applied in the proposed framework, namely the initial calibration and fouling calibration processes. The initial calibration was performed based on operational data obtained from the HP manufacturer. Here, the HP was tested under controlled conditions before it was delivered to the end user and thereby fouling was not present. The fouling calibration was based on operational data obtained from the SCADA system through the API. The specific period used for fouling calibration could be selected by the user and should represent periods where is required to analyse the effects of fouling on the HP. In this study, two different operational days were used for fouling calibration, one day before and one day after the CIP implementation. The initial and fouling calibration were comprised of an optimization process where the parameters shown in Table 1 were adjusted. This process minimized the normalized root mean square error (NRMSE) between measured and simulated outputs of interest or calibration targets over a period n, as shown in Eq. (5) and Eq. (6). The normalization was performed through the mean of the measured calibration target over a period n ($\overline{\mathrm{Target}}$). Multiple targets were used in a single optimization process, where each CT was

related to a specific weight (w). The targets for the initial calibration were $\dot{Q}_{sink}$, the total power intake from both compressors ($\dot{W}_{total}$) and the evaporation pressure (p_e), with weights equal to 33.3 % for each target. For the fouling calibration, the targets were the source pressure drop in the evaporator (dp_{eva}) and p_e, where each one had weights equal to 50 %. The weights were determined heuristically were all targets where assumed to have the same relevance.

Table 2: Parameters calibrated in the initial and fouling calibration processes.

Calibration process	Calibration parameter	Symbol	Variation range	Unit
Initial	Correction factor for DSH U-value	CF_{DSH}	0.3 to 1.7	[-]
	Correction factor for condenser U-value	CF_{con}	0.3 to 1.7	[-]
	Correction factor for SC U-value	CF_{SC}	0.3 to 1.7	[-]
	Correction factor for evaporator U-value	CF_{eva}	0.3 to 1.7	[-]
Fouling	Fouling-related evaporator thermal resistance	$R_{th,f}$	0 to 0.02	[K/kW]
	Fouling-related evaporator pressure drop	dp_f	0 to 0.5	[bar]

$$\min f(\text{Parameter}) = \sum_{i=1}^{n} w_i \cdot \text{NRMSE}_i \quad (5)$$

$$\text{NRMSE}_i = \overline{\text{Target}}_{\text{meas}}^{-1} \cdot \sqrt{n^{-1} \cdot \sum_{i=1}^{n} (\text{Target}_{\text{sim,i}}(\text{Parameter}) - \text{Target}_{\text{meas,i}})^2} \quad (6)$$

Time-invariant parameters were adjusted in the initial calibration, which corresponded to correction factors (CFs) for the overall heat transfer coefficients or U-values in the heat exchangers. In the fouling calibration, time-dependent parameters related to fouling were calibrated, namely $R_{th,f}$ and dp_f. The bounds for the calibrated parameters are shown in Table 2. The solution of Eq. (5) and Eq. (6) was obtained through the sequential least squares minimization algorithm available in the SciPy module in Python. The tolerances for both the initial calibration and the fouling calibration process were 10^{-5}.

3. Results

This section shows the results of the proposed monitoring framework, where the operation of the case study HP was monitored and analysed.

3.1. Simulated HP operation

Figure 4 and Figure 5 shows the time-series of the simulated and measured operational variables for a period of 19 days. The initial calibration reduced the difference between simulated and measured COP, $\dot{Q}_{sink}$ and p_e. This difference was reduced even further after the implementation of fouling calibration before the CIP. After the CIP was used, the fouling calibration process reduced the difference between the simulated and measured p_e, but not to the extent seen before the CIP. Moreover, the difference between simulated and measured $\dot{Q}_{sink}$ increased slightly after the second fouling calibration process. The results of the initial calibration process were probably not completely applicable for the period after the CIP, where the effects of fouling on the HP were low. Before the CIP, the mismatch between simulation and measured variables was likely to be lumped into the evaporator thermal resistance attributed to fouling. Regarding the pressure drop in the source stream, only the fouling calibration processes before the CIP led to a higher correspondence between the simulated and measured dp_{source} compared to the period before calibration. This indicated that the CIP did not have a significant effect on the removal of the effect of fouling on the source stream pressure drop.

https://doi.org/10.52202/069564-0296

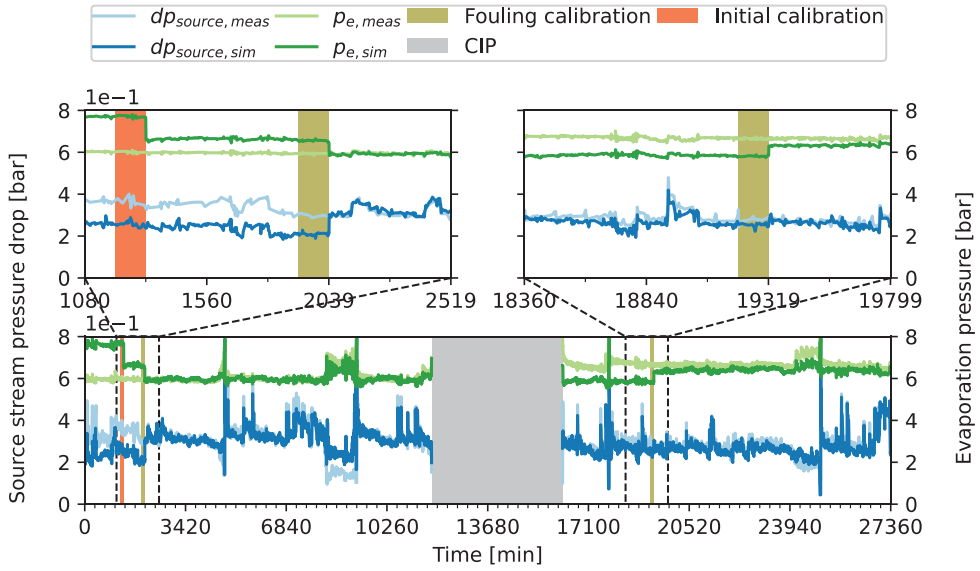

Figure 4: Time-series of the measured and simulated source stream pressure drop as well as evaporation pressure.

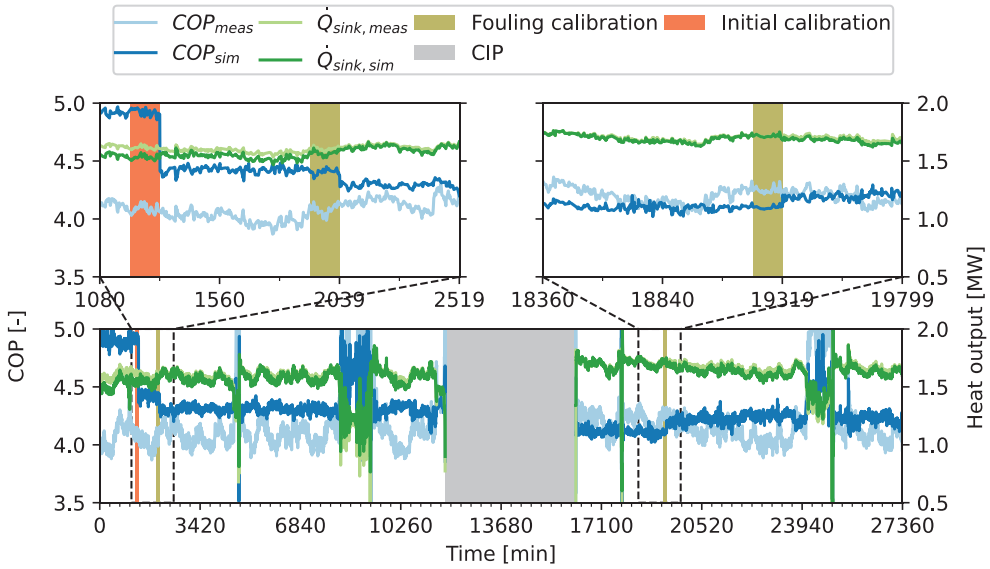

Figure 5: Time-series of the measured and simulated COP as well as heat output.

3.2. Residual analysis

The residuals shown in Figure 6 represent measured operational variables minus their respective simulated values. These residuals were not those presented in Section 2, as they were not normalized and were not used in the iteration processes for simulation (Figure 2) or calibration (Figure 3). The results from Figure 6 indicated that the fouling calibration implemented before the CIP period reduced the absolute value of the residuals related to dp_{eva}, p_e, $\dot{Q}_{sink}$ and $\dot{W}_{total}$. This was also valid for the fouling calibration applied after the CIP, except for dp_{eva}, which did not change significantly as a result of such a calibration. This was possibly an indication the CIP did not have a significant effect over the pressure drop caused by fouling. The initial calibration was observed to have a larger effect on the reduction of the discrepancies between measured and simulated values of COP and $\dot{W}_{total}$. This was expected given that the correction factors for the UA-values were calibrated in the initial calibration process. This led to an improved estimation of the pressure levels in the HP and thereby the total power intake from the compressors. The residuals shown in Figure 6 also showed that the dynamic behaviour of the case study HP was not completely represented by the simulation model. This was observed by the biased patterns in the residuals from the p_e, $\dot{Q}_{sink}$, COP and $\dot{W}_{total}$, which can be seen in Figure 6 at around 8000 min and 24000 min of operation.

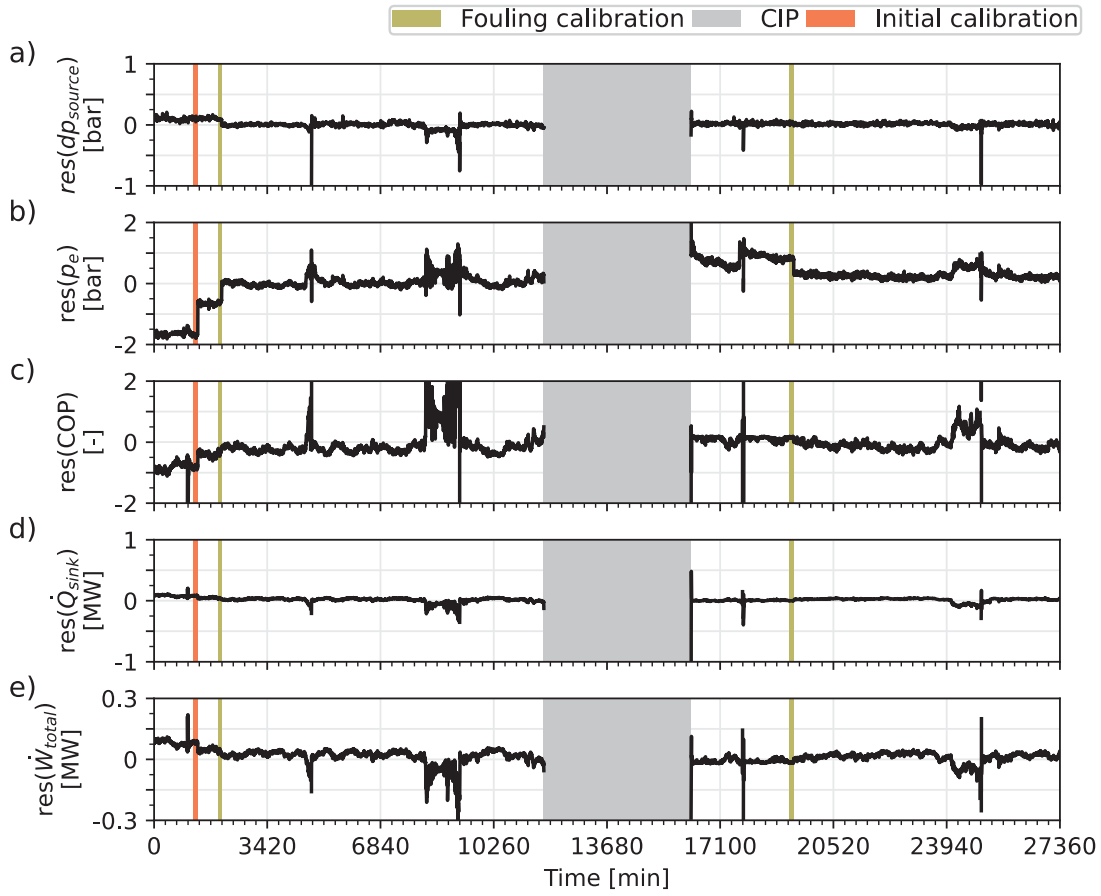

Figure 6: Residuals between simulated and measured operational variables of the HP.

3.3. Calibration results

Table 3 shows the parameters obtained from the calibration processes illustrated in Figures 4, 5 and 6. The calibration results of the correction factors showed that the U-values of the condenser, SC and evaporator presented in Table 1 were over-estimated, whereas they were underestimated for the DSH. This may also relate to a disagreement between the design and actual flow velocities as well as the temperature difference at the pinch point, which was assumed to be 5 K (see Table 1). The correction factors for the other heat exchangers were not significantly adjusted. The results showed that the $R_{th,f}$ and dp_f were reduced significantly as a result of the CIP (around 41 % and 100 %, respectively). However, the value of dp_f represented only around 15 % of the total source stream pressure drop shown in Figure 4. This was in agreement with the limited effect that the fouling calibration had on the calibration of the total source stream pressure drop, observed from the residual analysis shown in Figure 6.

Table 3: Parameters obtained from the calibration processes

Calibration process	Calibration parameter	Symbol	Result value	Unit
Initial	Correction factor for DSH U-value	CF_{DSH}	1.12	[-]
	Correction factor for condenser U-value	CF_{con}	0.96	[-]
	Correction factor for SC U-value	CF_{SC}	0.36	[-]
	Correction factor for evaporator U-value	CF_{eva}	0.47	[-]
Fouling (before CIP)	Fouling-related evaporator thermal resistance	$R_{th,f}$	$2.2 \cdot 10^{-3}$	[K/kW]
	Fouling-related evaporator pressure drop	dp_f	0.09	[bar]
Fouling (after CIP)	Fouling-related evaporator thermal resistance	$R_{th,f}$	0	[K/kW]
	Fouling-related evaporator pressure drop	dp_f	0	[bar]

https://doi.org/10.52202/069564-0296

4. Discussion

The automatic calibration method from the proposed framework reduced the discrepancy between the simulated and measured evaporation pressure, COP, heat output and source pressure drop (see Figures 4, 5 and 6). The results also indicated that the influence of fouling over the source stream pressure drop was significantly lower than the effect over the evaporator thermal resistance and that the CIP implementation led to a larger reduction of the latter than the former.

The relatively short simulation time used by the model applied in this study (around 10 seconds for the simulation of one hour) suggested its applicability for operation and fouling monitoring in a large-scale heat pump on a real-time basis. However, this would require the periodic verification of the validity of multiple factors that affect the simulation and calibration processes. These factors include the tolerances defined for the iteration residuals, the initial guess values and variation ranges for the calibration parameters, the optimization algorithm for NRMSE minimization, the selected calibration targets as well as the size and variability of the time-series data used for calibration. Those factors should be such that the best compromise is found between the required calculation time for calibration and the difference between simulation and measured data.

The results obtained from the proposed framework did not provide an estimation of the amount of deposited material on the heat transfer surface of the evaporator. This can be estimated with dedicated sensing devices for fouling examination such as ultrasonic probes [13] or infrared thermography equipment [14], which are unlikely to be available in large-scale HPs. In this context, the proposed model-based monitoring framework leverages existing sensing devices such as pressure and temperature sensors in the evaporator to estimate the effects of fouling. However, the results from the proposed monitoring framework were not contrasted with measurements from dedicated sensing devices for fouling characterization. This represents an opportunity for future studies.

The disagreements between the outputs of the model and the measured operational variables were probably lumped into the parameters adjusted in the calibration processes. For example, the difference between the heat transfer area of the heat exchangers in the model and in the case study HP was possibly included in the correction factors for the U-values in the model. Moreover, the assumption that those correction factors were calibrated based on an operational period when the evaporator was not affected by fouling due to the CIP usage, was not necessarily correct. Ideally, the initial calibration process should be based on an operational period right after fouling has been completely removed from the evaporator. In the present study, the correction factors obtained from the initial model calibration were also likely to include discrepancies between the model and the HP due to fouling. However, the evaporator of the case study HP could not be dismantled for cleaning, which prevented the complete removal of fouling.

The model used in this study led to a suboptimal representation of the dynamic off-design operation of the HP, which was indicated by the biased patterns observed in the simulation residuals (see Figure 6). It would require the use of a dynamic model to capture most of the dynamics present in a HP. The development of a dynamic simulation model may require information about the volumes and materials of the vessels, control-related parameters, refrigerant charge estimations as well as heat transfer and pressure drop correlations. The development of a quasi-steady-state model does not require such a comprehensive description about the design of a HP. Moreover, the present study focused on fouling monitoring, which often affects the operation of a HP at a slower rate than abrupt faults like the presence of condensed refrigerant in the suction line of a compressor.

The pumps in the secondary streams of the HP were not included in the simulation model. It is expected that the simulation residuals related to the estimation of power intake of such pumps will be reduced after the proposed fouling calibration framework is implemented. Modelling of the pumps could also indicate how the source side pressure drop affects the mass flow rate in the source stream. However, this adds complexity to the model, which may increase the time required for each simulation. Another limitation of the proposed framework was that it only enabled the analysis of historical data from the HP. The authors expect to complement the present version of the framework with forecasting methods that will enable the estimation of the future operation of a HP and the optimization of the time of CIP.

5. Conclusion

A quasi-steady-state simulation model of a heat pump used for district heating supply was calibrated based on operational data obtained from a cloud-based data management system. This framework enabled the estimation of the performance and the effects of fouling on the heat pump, even when the model did not represent accurately the dynamics of such a system. Particularly, the re-calibration of the model based on time-dependant parameters related to fouling allowed to obtain simulation results that were in agreement with measurements over a period of nearly three weeks. This allowed to assess the degree to which a CIP implementation reduced the evaporator thermal resistance and source stream pressure drop caused by fouling. The proposed framework could be used for real-time monitoring of large-scale heat pumps, where the relatively short simulation time achieved, automatic model calibration and leverage of existing sensing devices could be beneficial.

Acknowledgments

This work was funded by EUDP (Energy Technology Development and Demonstration) under the project "Digital twins for large-scale heat pump and refrigeration systems" (project number: 64019-0570).

Nomenclature

Abbreviations

API	application programming interface
CF	correction factor
CIP	cleaning-in-place
HP	heat pump
HS	high-stage
LS	low-stage
(N)RMSE	(normalized) root mean square error
res	residual
SCADA	supervisory control and data acquisition

Letter symbols

A	heat transfer area, m^2
dp	pressure difference, bar
dT	temperature difference, K
$\dot{m}$	mass flow rate, kg/s
N	compressor speed, rpm
$\dot{Q}$	heat flow rate, kW
p	pressure, bar
R	thermal resistance, K/kW
T	temperature, ˚C
U	overall heat transfer coefficient, kW/Km^2
V	volume, m^3
$\dot{V}$	volume flow rate, m^3/s
w	weight, -
$\dot{W}$	power, kW

Greek symbols

ρ	density, kg/m^3
η	efficiency, -

Subscripts and superscripts

c	condensation
calc	calculated
clean	clean
con	condenser
DSH	desuperheater
meas	measurement
e	evaporation
eva	evaporator
f	fouling
h	heat output
in	inlet
is	isentropic
m	intermediate
out	outlet
pp	pinch-point
s	swept
sc	sub-cooler
sim	simulation
sink	sink stream
sp	set point
source	source stream
total	total
th	thermal
vol	volumetric
w	water

References

[1] IEA. The future of heat pumps [Internet]. Paris, France; 2022. Available from: https://www.iea.org/reports/the-future-of-heat-pumps

[2] Aguilera JJ, Meesenburg W, Ommen T, Poulsen JL, Kramer KR, Markussen WB, et al. Operational challenges in large-scale ammonia heat pump systems. In: Proceedings of ECOS 2021: 34th International Conference on Efficiency, Cost, Optimization, Simulation and Environmental Impact of Energy Systems. Taormina, Italy; 2021. p. 12.

[3] Aguilera JJ, Meesenburg W, Ommen T, Markussen WB, Poulsen JL, Zühlsdorf B, et al. A review of common faults in large-scale heat pumps. Renew Sustain Energy Rev [Internet]. 2022 Oct 1 [cited 2022 Aug 18];168:112826. Available from: https://10.0.3.248/J.RSER.2022.112826

[4] Bott TR. Fouling of heat exchangers [Internet]. Amsterdam, The Netherlands: Elsevier Science B.V.; 1995. 524 p. Available from: https://doi.org/10.1016/B978-0-444-82186-7.X5000-3

[5] Pogiatzis T, Ishiyama EM, Paterson WR, Vassiliadis VS, Wilson DI. Identifying optimal cleaning cycles for heat exchangers subject to fouling and ageing. Appl Energy [Internet]. 2012 Jan 1 [cited 2023 Mar 24];89(1):60–6. Available from: https://doi.org/10.1016/j.apenergy.2011.01.063

[6] Meesenburg W, Aguilera JJ, Kofler R, Markussen WB, Elmegaard B. Prediction of fouling in sewage water heat pump for predictive maintenance. In: Proceedings of ECOS 2022: 35th International Conference on Efficiency, Cost, Optimization, Simulation and Environmental Impact of Energy Systems. Copenhagen, Denmark; 2022. p. 12.

https://doi.org/10.52202/069564-0296

[7] Aguilera JJ, Andreas S, Meesenburg W, Ommen T, Markussen WB, Zühlsdorf B, et al. Integration of dynamic model and classification methods for fault detection and diagnosis in a chiller. In: 15th IIR-Gustav Lorentzen conference on Natural Refrigerants [Internet]. Trondheim, Norway; 2022. p. 14. Available from: https://10.0.72.30/iir.gl2022.96

[8] Cui J, Wang S. A model-based online fault detection and diagnosis strategy for centrifugal chiller systems. Int J Therm Sci [Internet]. 2005 Oct 1 [cited 2021 Jun 14];44(10):986–99. Available from: https://10.0.3.248/j.ijthermalsci.2005.03.004

[9] Vering C, Borges S, Coakley D, Krützfeldt H, Mehrfeld P, Müller D. Digital twin design with on-line calibration for HVAC systems in buildings. In: Building Simulation Conference 2021: 17th Conference of IBPSA. Bruge, Belgium; 2021.

[10] Jonas Klingebiel, Göbel S, Venzik V, Mueller D. Evaluation of machine learning methods for optimizing the defrosting process of air-to-water heat pumps. In: 15th IIR-Gustav Lorentzen conference on Natural Refrigerants [Internet]. Trondheim, Norway; 2022. p. 12. Available from: https://10.0.72.30/iir.gl2022.0117

[11] Virtanen P, Gommers R, Oliphant TE, Haberland M, Reddy T, Cournapeau D, et al. SciPy 1.8.0: Fundamental algorithms for scientific computing in Python. Nat Methods [Internet]. 2020;17(3):261–72. Available from: https://doi.org/10.1038/s41592-019-0686-2

[12] Bell IH, Wronski J, Quoilin S, Lemort V. Pure and Pseudo-pure Fluid Thermophysical Property Evaluation and the Open-Source Thermophysical Property Library CoolProp. 2014; Available from: https://10.0.3.253/ie4033999

[13] Bott TR. Biofouling Control with Ultrasound. Heat Transf Eng [Internet]. 2010;21(3):43–9. Available from: https://www.tandfonline.com/action/journalInformation?journalCode=uhte20

[14] Berce J, Zupančič M, Može M, Golobič I. Infrared thermography observations of crystallization fouling in a plate heat exchanger. Appl Therm Eng [Internet]. 2023 Apr 1 [cited 2023 Mar 24];224:120116. Available from: https:///J.APPLTHERMALENG.2023.120116